Airborne Measurements of Wave Growth for Stable and Unstable Atmospheres in Lake Michigan[1]

PAUL C. LIU

Great Lakes Environmental Research Laboratory, NOAA, Ann Arbor, MI 48104

DUNCAN B. ROSS

Sea-Air Interaction Laboratory, NOAA, Miami, FL 33149

(Manuscript received 18 March 1980, in final form 28 July 1980)

ABSTRACT

This paper presents the results of a joint program combining airborne laser profilometer and Waverider buoy measurements of synoptic wave conditions in Lake Michigan during the passage of an intense cold front. Measurements were made both before and after passage of the front under different atmospheric stabilities. The results demonstrate the distinctive role stability plays in wave growth processes. Specifically, it is evident that the wind speed and fetch distance required to generate the same wave conditions are less for an unstable atmosphere than for a stable atmosphere. Therefore, an unstable atmosphere is usually accompanied by higher waves for the same 10 m winds. Fetch-limited wave growth is seen to follow stable or unstable quasi-equilibrium relations between corresponding wave-energy and peak-energy frequency parameters. Synoptic wave height maps for Lake Michigan have been prepared from the measured data.

1. Introduction

Airborne wave measurements made from low-flying aircraft with radar or laser altimeters have generally been recognized as an effective means of providing useful data for practical applications. The experiment of Barnett and Wilkerson (1967) using a radar altimeter represents one of the earliest and best known attempts to use airborne measurements to examine the applicability of wave-growth theories. Similar measurements using a laser altimeter have been presented by Ross *et al.* (1970), Schule *et al.* (1971) and Ross and Cardone (1974). Perhaps one of the most advantageous features of airborne measurements yet to be fully explored is their ability to measure virtually synoptic conditions over large bodies of water, such as the Great Lakes. An earlier application using a radar altimeter over Lake Michigan was conducted by Wilkerson and Ropek (1967). Their data, however, were not analyzed.

In 1977 a program combining measurements by the airborne laser altimeter with buoy measurements was undertaken jointly by the Great Lakes Environmental Research Laboratory (GLERL) and the Sea-Air Interaction Laboratory of NOAA in Miami, Florida. The purpose was to measure synoptic wave conditions in Lake Michigan during an autumn storm. Since Waverider buoys record lake-truth data that represent wave conditions at a single location, and the intricate boundary configuration and island chains of the Great Lakes render single-location data ineffective in generalizing lakewide conditions, this observational program was particularly valuable to ascertain the lake-wide spatial variability of waves as measured by airborne lasers. This paper describes the program and gives the results of data analysis that led to the development of synoptic Lake Michigan wave-height maps during the storm, as well as detailed examinations of fetch-limited spatial growth of spectral wave components and their correlations with the parameterized dynamic growth processes.

2. The experiment

a. Instrumentation

The airborne measurements were made from a NOAA C-130 aircraft instrumented with a Spectra Physics Geodolite laser altimeter to profile the lake surface, an inertial navigation system to measure wind speed and direction, and a Barnes PRT-5 radiometer to measure sea surface temperature. The aircraft flew at a speed of 106 m s^{-1} at 150 m above the lake surface parallel to the direction of the wind. Since this speed was considerably greater than the speed of the longest waves, the measured wave

[1] GLERL Contribution No. 208.

profile closely represented an instantaneous traverse of the lake surface along the line of flight. The effects of aircraft motion on the measurements were removed by a high-pass filter. Detailed discussions of the instrumentation and measurements from the aircraft are given by Ross *et al.* (1970) and Ross (1978).

The *in situ* wave measurements were made from two Waverider buoys deployed at a water depth of 150 m, 20 km offshore from Muskegon, Michigan, and Milwaukee, Wisconsin, respectively. The Waverider buoy, manufactured by Datawell, Holland, is of spherical shape, 1 m in diameter and weighs 100 kg. Its main component is an accelerometer mounted on a pendulous system to measure the vertical component of acceleration, which is double integrated electronically to yield the vertical displacement. The wave signal is telemetered to a shore receiver and recorded continuously on magnetic tapes. The recording system is described by Liu and Robbins (1974).

b. Operation prediction

Because the NOAA aircraft is stationed at Miami, accurate prediction of the intensity and track of a developing low pressure system was required. The procedure established gave aircraft personnel 48 h notice of the proper conditions. The alert was confirmed or cancelled 24 h later. The aircraft then left Miami 4–5 h before the start of a measurement program on Lake Michigan. Forecasting support was requested from and provided by the National Weather Service (NWS) Forecast Office in Chicago. From October to November 1977 constant daily contact occurred between GLERL and the Chicago Forecast Office to keep abreast of any storm situation developing over Lake Michigan, and to obtain their initial prognosis and subsequent updates. The expected storm situation would be the passage of a cold front over the lake that generates 10–15 m s^{-1} wind speed on both sides of the front.

c. The episode

An alert was called on 18 November when a low pressure center started to form over the Colorado area. It was confirmed the next day, when the low deepened and moved northeast. On 20 November, the day of the first flight, the center was located over the Northern Plains area and provided strong, uniform southerly winds over Lake Michigan. The front moved across the Lakes during the evening, and on 21 November, when the low pressure was situated south of Hudson Bay and was generating predominately west winds over Lake Michigan, a second measurement flight was made. Two 1500 GMT weather maps for these two days are shown in Fig. 1. Fig. 2 presents the tracks covered by the two flights, each lasting ~5 h. The closed circles

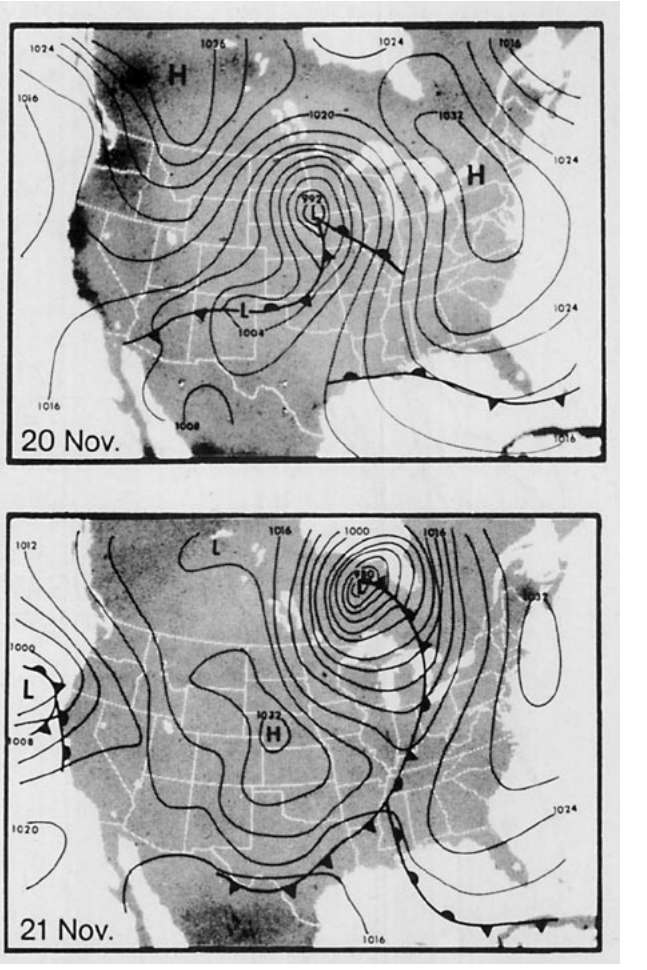

FIG. 1. 1500 GMT weather maps for 20 and 21 November 1977.

shown in Fig. 2 indicate the location of GLERL Waverider buoys.

3. Treatment of data

The airborne wave measurements were made continuously along the flight tracks and recorded on a multichannel FM tape recorder. Segments of lake-surface profile for each 2 min of data were digitized at an interval of ~0.06 s. After high-pass filtering the data to remove aircraft motion effects, raw wave spectra were calculated with fast Fourier transforms. By making transformations that map the spectra from a moving to a fixed coordinate system one can retrieve estimates of one-dimensional frequency wave spectra (Barnett and Wilkerson, 1967). The calculations were made with 45 degrees of freedom. Following the flight tracks shown in Fig. 2, a total of 63 and 51 frequency spectra were obtained for the 20 and 21 November flights, respectively. For each of the spectra, significant wave height, peak-energy frequency, average surface wind speed and direction, and surface air and

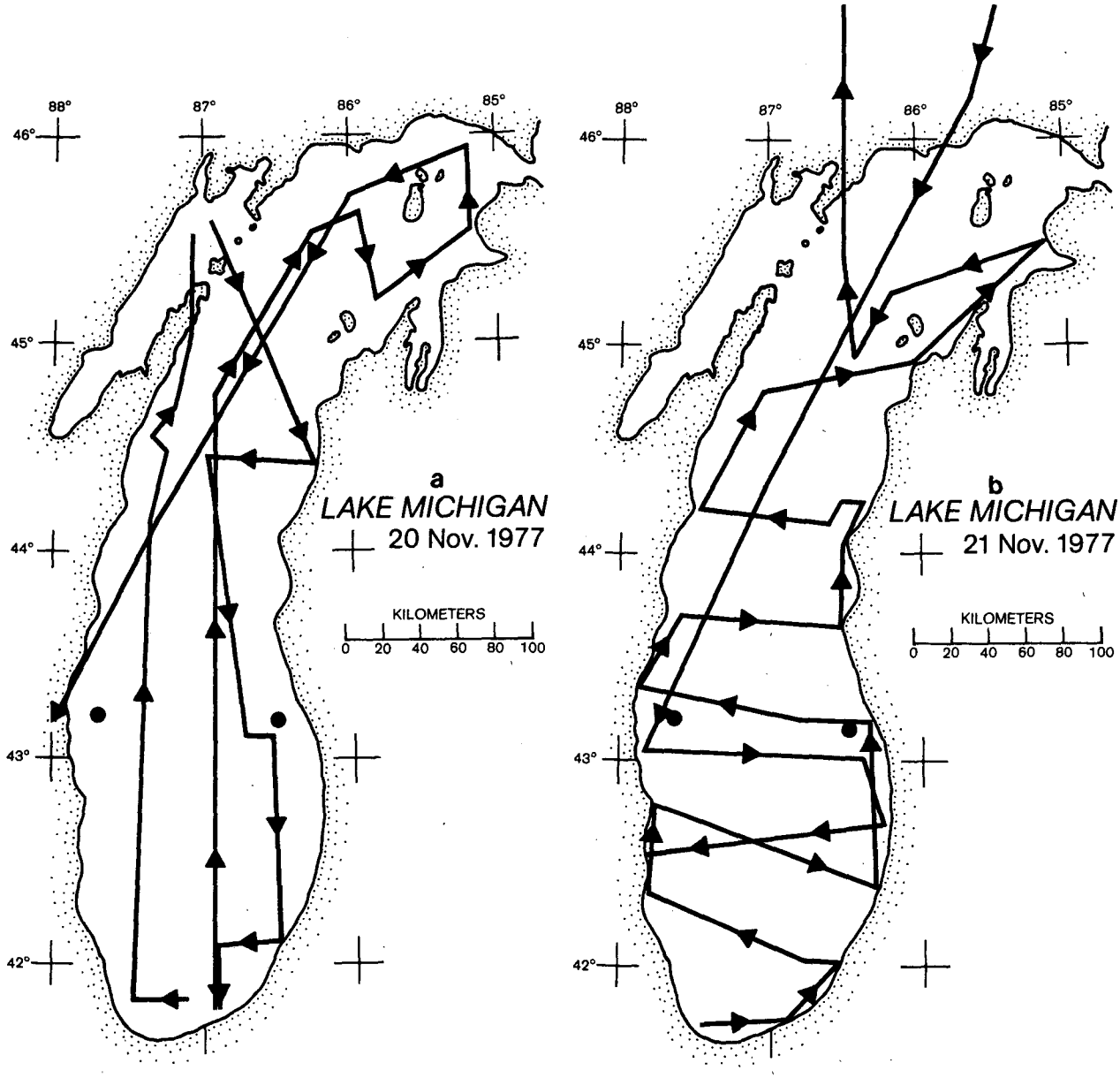

FIG. 2. Flight tracks over Lake Michigan made during (a) 20 November and (b) 21 November 1977.

water temperature were also obtained for further analysis. Surface winds were calculated from measurements of 150 m flight level winds by the aircraft's inertial navigator-based system. The calculations involved use of the boundary-layer model of Cardone (1969), which incorporates a parameterization of the stability effect on the wind profile, to extrapolate equivalent 10 m level winds.

The wave data recorded from the Waveriders on magnetic tapes were digitized at ⅓ s sampling intervals. To facilitate comparisons with airborne data analysis, data from a continuous 30 min record at 1 s sampling intervals were used for calculating wave-frequency spectra. Because of noise interference, only five and six spectra during the respective 20 and 21 November flights were available for comparison. Both the Blackman and Tukey (1958) and fast Fourier transform methods were used in the calculations, with 120 and 60 degrees of freedom, respectively. The spectra calculated by the two methods were practically identical. In the following analysis Blackman and Tukey results were used.

Since there were no simultaneous wind measurements available at the Waverider locations during the two days when airborne measurements were made, corresponding overlake wind data were de-

duced and interpolated from the overland wind data recorded at the nine NWS Coastal Marine Stations around Lake Michigan.

4. Results and discussion

a. Data intercomparisons

Since Waverider data represent the "lake truth," a direct comparison between laser and Waverider measured spectra would be of immediate interest. As can be seen in Fig. 2, there were three instances when the airplane track passed close to the Waveriders. The Waverider data for the period on 20 November, however, when the aircraft flew over the Muskegon-side Waverider, had to be discarded because of the interference of excessive noise. Therefore, only two Waverider spectra were available to compare with the corresponding laser spectra. Fig. 3 presents the two direct comparisons. Considering that 1) the spectra were obtained from a moving and a stationary coordinate system separately, 2) the Waverider data were less reliable at high frequencies, and 3) the spectral estimates are carrying 90% confidence limits of 0.78 and 1.28, the agreements shown in the figures are quite encouraging. The laser spectra, in general, can be regarded as consistent with the lake truth, and thus are useful estimates for further detailed analyses.

b. Parameter correlations

Correlating nondimensionalized wave parameters has been an effective way of examining the characteristics of observed data. Many recent studies, following the scaling relations suggested by Kitaigorodskii (1962), have found that fetch-limited wave parameters, when nondimensionalized with wind speed U_{10} and gravitational acceleration g, are functions of the nondimensional fetch parameter $\xi = gX/U_{10}^2$, where X is the fetch distance. Their functional forms vary, however, among different studies. For instance, the JONSWAP relations developed by Hasselmann *et al.* (1973) describe the fetch dependence of the nondimensional peak-energy frequency $\nu = U_{10}f_m/g$ and nondimensional total energy $\epsilon = Eg^2/U_{10}^4$, respectively, by

$$\nu = 3.5\xi^{-0.33} \tag{1}$$

and

$$\epsilon = 1.6 \times 10^{-7}\xi, \tag{2}$$

where for a given wave-energy-density spectrum $S(f)$, f_m is the peak-energy frequency and $E = \int S(f)df$ is the measure of total energy per unit surface area with the constant factor ρg left out.

Relation (1) was developed by synthesizing field and laboratory wave data. Contending that the

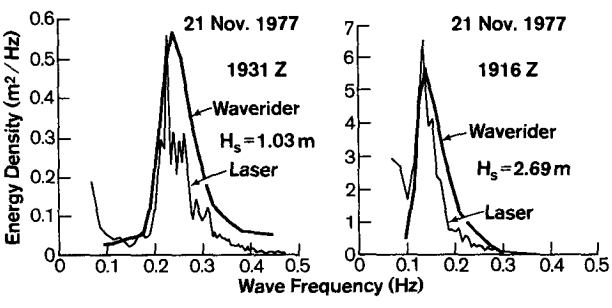

FIG. 3. Comparisons of corresponding wave spectra obtained from a laser altimeter and from a Waverider buoy.

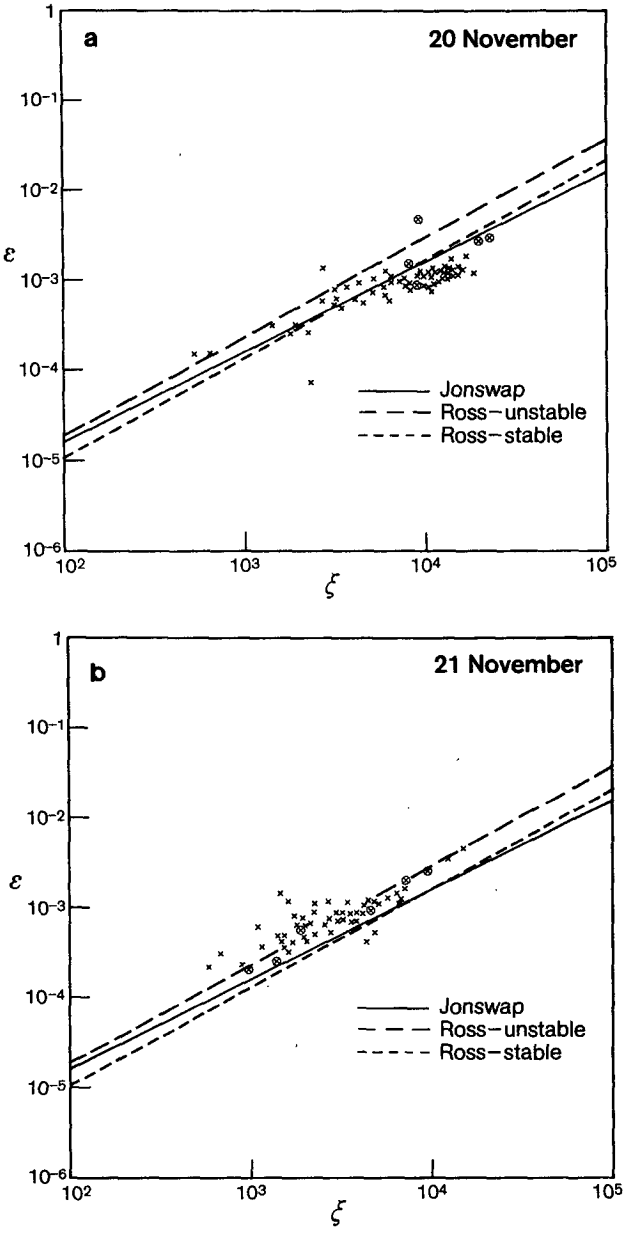

FIG. 4. Correlating (a) ϵ vs ξ and (b) ν vs ξ relations for 20 November data.

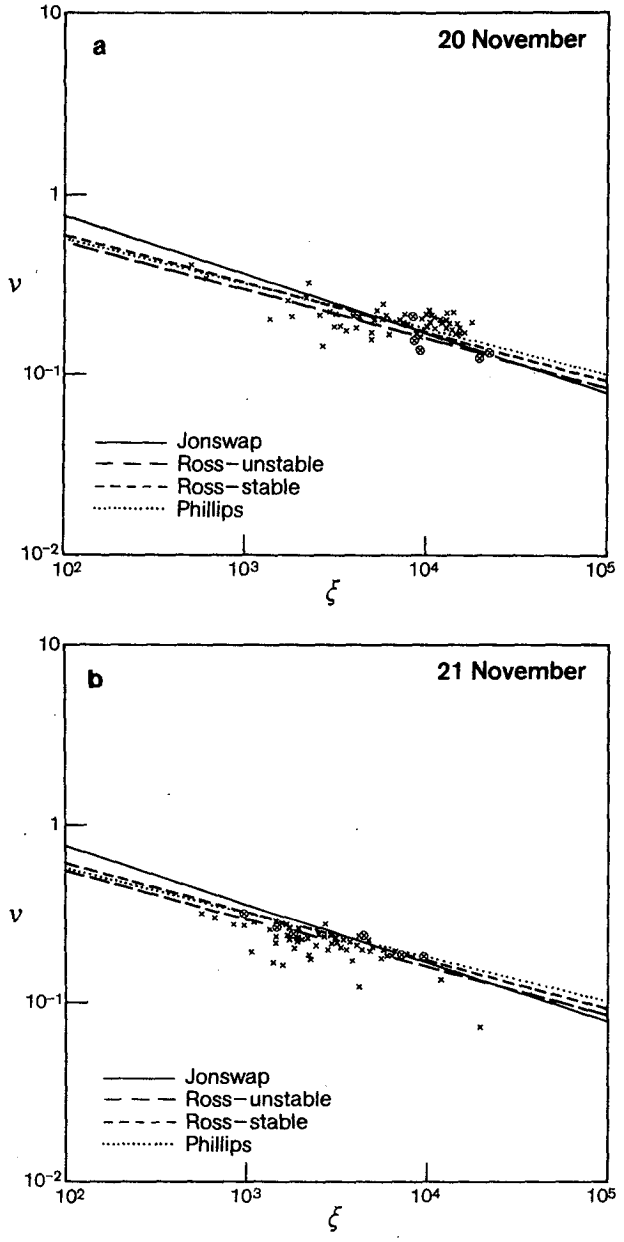

FIG. 5. As in Fig. 4 except for 21 November data.

dynamical processes in laboratory measurements are different from those in the field, Phillips (1977) disregarded the laboratory measurements and found that a relation more compatible with Eq. (2) is

$$\nu_P = 1.78\xi^{-1/4}. \quad (3)$$

Ross (1978), on the other hand, combined airborne measurements from the North Sea with those from the western Atlantic Ocean and found the relations to be

$$\nu_{RU} = 1.9\xi^{-0.27} \quad (4)$$

and

$$\epsilon_{RU} = 1.2 \times 10^{-7}\xi^{1.1}. \quad (5)$$

The use of subscripts U in these relations indicates that they are for unstable atmospheric conditions that will be discussed later. Comparisons of these relations with the data obtained from the present study are shown in Figs. 4 and 5 for the data collected 20 and 21 November, respectively. All available Waverider data during the corresponding flights were included in these figures as shown by the circled points. Each of these figures contains both ϵ vs ξ and ν vs ξ, relations presented as parts (a) and (b), respectively. Corresponding relationships (1)–(5) are plotted for comparison. Examination of these figures shows the data points generally scattered around the empirical relations from the other studies. Distinctive differences, however, exist between the 20 November data and those of 21 November. For ϵ vs ξ relations, the figures clearly show that the 20 November data fit the JONSWAP relation (1), whereas the 21 November data fit Ross's relation (5). For ν vs ξ relations the distinction is less clear, but the 20 November data appear to fit Ross' relation (4) better, especially in the region $\xi < 10^4$ where growth was observed, while the 21 November data seem to fit Phillips's relation (3) better. This distinction is of particular interest, since on 20 November, prior to passage of the cold front over Lake Michigan, the surface boundary layer was stable, with a measured air-water temperature difference that varied from +2 to +4°C. On 21 November, on the other hand, the atmospheric boundary layer behind the front was unstable, with an estimated air-water temperature difference of −8°C. Therefore, the results show that the processes are affected qualitatively by the atmospheric stability.

Noting that Ross' relations (4) and (5), which fit well with the 21 November data under unstable atmospheric conditions, were indeed obtained under a clearly unstable atmosphere, we regard (4) and (5) as being appropriate to unstable conditions, and de-

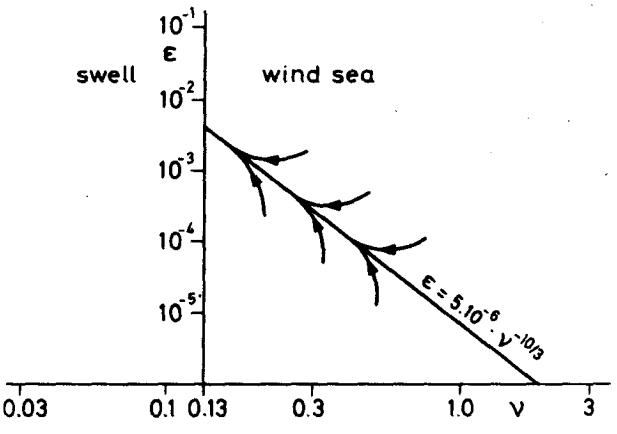

FIG. 6. Wave growth in the ϵ vs ν plane (after Hasselmann *et al.*, 1976).

TABLE 1. Data summary for the five growth episodes shown in Figs. 7–11.

NO.	TIME GMT	LAT. DEG.N	LONG. DEG.W	FLIGHT LEVEL ALTITUDE M	FLIGHT LEVEL WIND SPEED M/S	FLIGHT LEVEL WIND DIRECT. DEG.	FLIGHT LEVEL AIR TEMP. C	SURFACE 10M WIND SPEED M/S*	SURFACE 10M WIND DIRECT. DEG.*	SURFACE AIR TEMP. C	FRICTION VELOCITY M/S*	WATER TEMP. C	SIGNIFICANT WAVE HT. M	PEAK FREQUENCY HZ
	NOVEMBER 20, 1977													
1	1740	41.9	87.4	120.2	19.8	190	11.7	12.5	190	11.8	.52	10.3	1.00	.200
2	1742	42.1	87.4	127.3	19.2	187	10.5	13.8	189	11.8	.49	10.4	1.24	.186
3	1750	42.5	87.4	131.1	22.0	189	10.5	13.4	188	11.8	.53	9.5	1.72	.155
4	1753	42.7	87.4	142.5	20.8	184	9.9	13.2	186	11.3	.49	9.3	1.70	.154
5	1755	42.9	87.4	414.6	20.8	182	9.6	13.0	183	11.0	.50	9.1	1.99	.144
6	1758	43.1	87.4	147.6	20.6	182	9.1	13.7	182	10.5	.54	9.3	2.14	.133
7	1801	43.2	87.5	149.6	21.3	181	9.0	13.5	182	10.5	.53	8.9	2.51	.122
8	1803	43.4	87.5	149.7	20.7	179	8.9	14.0	179	10.4	.56	9.3	2.36	.142
9	1806	43.6	87.5	152.0	19.5	177	8.8	13.5	178	10.3	.48	8.9	2.28	.132
10	1809	43.7	87.5	151.5	20.3	174	8.6	12.3	175	10.1	.46	8.3	2.30	.133
11	1811	43.9	87.5	152.8	19.9	169	8.2	12.1	171	9.7	.44	7.9	2.58	.133
12	1814	44.0	87.5	148.5	20.2	165	8.1	13.5	167	9.6	.54	8.5	2.67	.137
13	1816	44.2	87.4	137.6	20.1	169	8.0	13.2	169	9.4	.54	8.3	2.40	.124
14	1819	44.3	87.4	140.1	20.3	171	8.0	14.1	170	9.4	.58	8.6	2.75	.123
15	1821	44.5	87.4	140.4	20.4	164	8.0	14.9	167	9.4	.57	8.4	3.11	.125
	NOVEMBER 20, 1977													
2	2022	42.2	87.0	121.5	21.1	187	11.8	11.9	187	13.0	.41	9.1	1.43	.173
3	2025	42.4	87.0	128.2	21.4	188	11.2	12.4	187	12.5	.49	9.9	1.68	.156
4	2027	42.6	87.0	142.2	22.4	185	10.8	13.2	187	12.1	.48	9.3	1.81	.153
5	2030	42.8	87.0	147.3	23.3	185	10.6	13.0	185	12.1	.52	9.3	2.16	.150
6	2032	43.0	87.0	148.8	22.7	183	10.2	13.5	184	11.7	.50	9.0	2.23	.142
7	2037	43.3	86.9	149.1	22.7	181	9.9	13.1	182	11.4	.49	8.5	2.48	.134
8	2039	43.5	86.9	150.6	23.7	181	9.7	13.7	181	11.2	.52	8.2	2.78	.134
9	2044	43.9	86.9	155.1	24.3	183	9.6	14.9	182	11.2	.58	8.7	3.03	.131
10	2048	44.1	86.9	151.3	24.5	181	9.4	15.7	182	10.9	.66	9.1	2.88	.132
11	2050	44.2	86.9	161.4	24.1	181	9.2	15.9	181	10.7	.63	9.0	3.17	.131
12	2053	44.4	86.9	176.2	23.2	181	8.9	14.9	181	10.6	.55	8.8	3.00	.138
13	2055	44.6	86.9	180.2	22.7	182	8.6	14.3	182	10.4	.56	8.9	3.06	.117
14	2058	44.7	86.9	193.6	23.1	182	8.4	15.0	182	10.2	.60	8.9	3.13	.117
15	2106	45.2	86.6	203.6	22.9	178	8.5	14.8	180	10.5	.54	9.0	3.10	.127
	NOVEMBER 21, 1977													
1	1847	42.9	87.6	148.8	13.4	274	-2.4	12.2	275	-.9	.50	7.8	.84	.227
2	1850	42.8	87.4	151.9	14.7	283	-2.2	12.6	281	-.7	.55	7.8	1.43	.182
3	1852	42.8	87.2	147.7	14.1	281	-1.8	12.8	283	-.4	.53	7.7	2.24	.160
4	1855	42.7	86.9	141.3	13.9	284	-1.5	12.8	282	-.1	.52	8.4	2.26	.153
5	1857	42.7	86.7	139.8	15.1	286	-1.0	12.9	286	-.6	.56	8.6	2.45	.136
6	1900	42.7	86.5	141.1	14.5	284	-.8	13.3	287	-.4	.54	9.5	2.68	.136
	NOVEMBER 21, 1977													
1	1916	43.2	86.5	141.0	15.3	274	-1.7	13.4	276	-.3	.58	8.9	2.84	.136
2	1919	43.2	86.7	141.7	14.0	268	-1.7	12.7	272	-.3	.52	8.1	2.24	.155
3	1921	43.2	86.9	144.8	14.1	265	-2.0	12.7	267	-.6	.53	7.7	2.20	.154
4	1924	43.2	87.1	149.1	12.8	269	-2.0	12.1	267	-.5	.47	7.5	1.76	.171
5	1927	43.2	87.3	145.7	13.7	259	-2.3	12.2	261	-.8	.51	7.5	1.65	.172
6	1929	43.2	87.5	146.7	13.3	263	-2.4	12.1	261	-1.0	.50	8.0	1.23	.210
7	1932	43.2	87.7	148.1	11.8	254	-2.7	12.0	258	-1.2	.44	7.5	.88	.230
	NOVEMBER 21, 1977													
1	2312	43.2	87.6	164.9	15.0	264	-3.0	13.1	263	-1.4	.56	6.3	1.23	.213
2	2315	43.2	87.3	161.8	15.4	263	-2.5	13.1	264	-.9	.57	5.8	1.58	.178
3	2318	43.2	87.1	155.8	15.4	267	-2.0	13.2	265	-.5	.57	6.3	1.90	.164
4	2320	43.2	86.8	159.3	14.8	264	-1.7	13.1	265	-.1	.55	7.1	2.31	.157
5	2323	43.2	86.6	164.9	15.7	272	-1.5	12.9	269	-.2	.58	7.7	2.14	.150

*: DATA WERE CALCULATED USING CARDONE(1969) MODEL

duce analogous relations to fit the 20 November data for stable conditions. This can be done by following Cardone's (1969) method, which employs stability dependence of the drag coefficient based on the Monin-Obukhov similarity theory to modify the curvature of wind profiles at the lake-atmosphere boundary layer. For a given friction velocity, the modification results in higher wind speeds at the

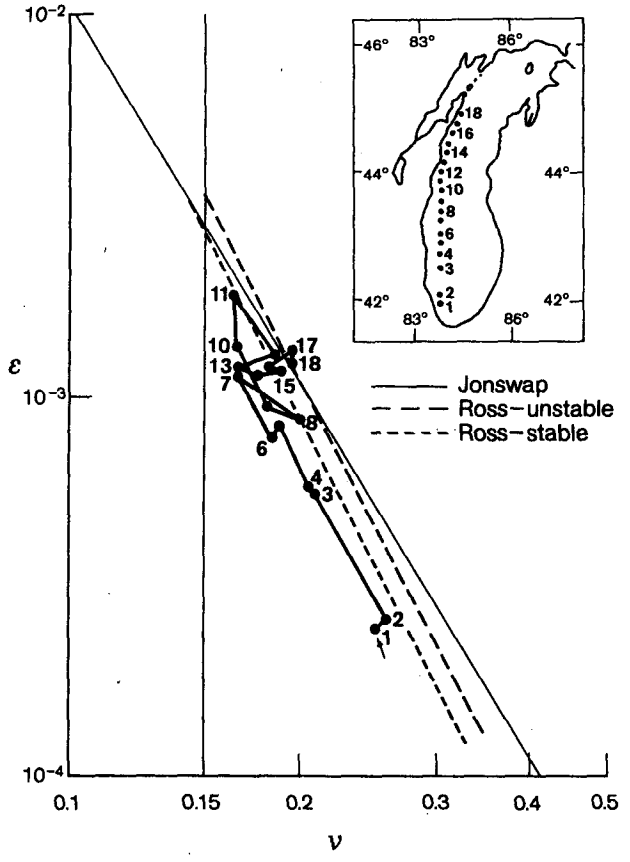

FIG. 7. An episode of wave growth in the ϵ vs ν plane from 1740 to 1821 on 20 November. The locations of measurement points are shown in the inserted map.

10 m level for stable conditions than would be observed under unstable or neutral conditions. Consequently, a stable Ross relation can be obtained by modifying the wind speeds in (4) and (5) to yield

$$\nu_{RS} = 2.05\xi^{-0.27}, \tag{6}$$

$$\epsilon_{RS} = 6.80 \times 10^{-8}\xi^{1.1}. \tag{7}$$

Relations (6) and (7), also plotted in Figs. 4 and 5, are obtained by increasing wind speed from unstable to stable atmosphere 19% in Eq. (4) and 27% in Eq. (5), respectively. The 19% speed increase, equivalent to a 30% reduction in drag coefficient, is consistent with Cardone's model for a +3°C air-water temperature difference. For the ϵ vs ξ relation in which the stability effect is most distinctive, further adjustment is necessary to fit the data better. This implies that the stability effect included in Cardone's model is weaker than the actual effect in the field in this case. Nevertheless, while it is not profound, these results represent a rational effort to quantify the well-known but elusive atmospheric stability effects.

c. *Process of wave growth*

Incorporating nonlinear energy transfer calculations into a parametric wave model, Hasselmann *et al.* (1976) derived a quasi-equilibrium relation for ϵ and ν given by

$$\epsilon = 5.1 \times 10^{-6}\nu^{-10/3} \tag{8}$$

as a first-order solution to their two-parameter prognostic equations. Note that an ϵ vs ν relation can be deduced directly from (1) and (2) with different coefficient and exponential values. Relation (8), shown in Fig. 6, has been used in numerical predictions (Hasselmann, 1978) as a model of equilibrium state for growing wind waves under a uniform wind field. As the waves grow, the equilibrium state migrates along the equilibrium line in the direction of lower frequencies and higher energies with increasing fetch or duration until the fully developed condition is reached ($\nu \approx 0.13$). According to this model, wave states that initially lie off the equilibrium line will be converging to it as shown by the characteristic curves. The airborne wave measurements taken during 20 and 21 November provided an ideal data set to examine this model directly.

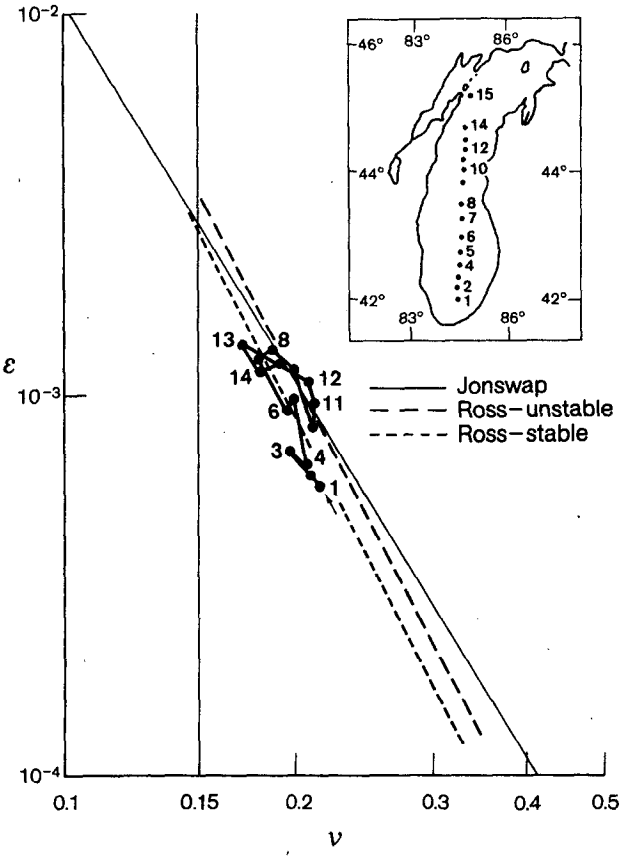

FIG. 8. As in Fig. 7 except for 2019–2106 on 20 November.

From the measurements there were five traverses made in the downwind or upwind direction, all of which were considered ideal wave growth episodes. A detailed data summary of these episodes is given in Table 1. The two traverses on 20 November, during a southerly wind, covered a fetch distance of ~300 km each. The three traverses on 21 November during a westerly wind across the lake, on the other hand, each covered approximately a fetch distance of 100 km. The five cases are presented in Figs. 7–11. For each case, there is a map to indicate the points of measurement along the traverse; the corresponding normalized data points are plotted on the ϵ vs ν plane. An arrow indicates the point for the shortest fetch, with each subsequent data point along the increasing fetch distance on the traverse connected by a thin line to show the sequence of wave field development. With the exception of Fig. 10, which was an upwind measurement, all measurements shown were made in the downwind direction.

An examination of these figures confirms that the waves are growing along an equilibrium line in the direction of lower frequency and higher energy. However, the three cases on 21 November appear to adapt closer to relation (8) than do the two cases on 20 November. Considering the differences in atmospheric stability during the two days, unstable and stable ϵ vs ν relations are deduced by eliminating ξ from Eqs. (4) and (5), and (6) and (7), respectively, such that

$$\epsilon_{RU} = 1.64 \times 10^{-6} \nu_{RU}^{-4.07}, \quad (9)$$

$$\epsilon_{RS} = 1.26 \times 10^{-6} \nu_{RS}^{-4.07}. \quad (10)$$

Plots of (9) and (10) on Figs. 7–11 show clearly that they provide better representations of wave growth for the corresponding unstable or stable conditions during the measurements.

The waves during the 21 November cases grew along the equilibrium relation (9), and the corresponding fetches were relatively shorter across the lake. For the episodes on 20 November with long fetches along the lake's longitudinal axis, on the other hand, the wave growth patterns were initially off the equilibrium line (10) and subsequently converged toward it. But the process of converging involves decreasing energy and increasing peak-energy frequency that leads to several loops toward the equilibrium line. The looping processes show no further migration along the equilibrium line beyond $\nu = 0.13$ or 0.15, the fully developed condition for an unstable or stable atmosphere according to Cardone's model. Thus the loops, being less than fully developed, appear to be part of the well-known,

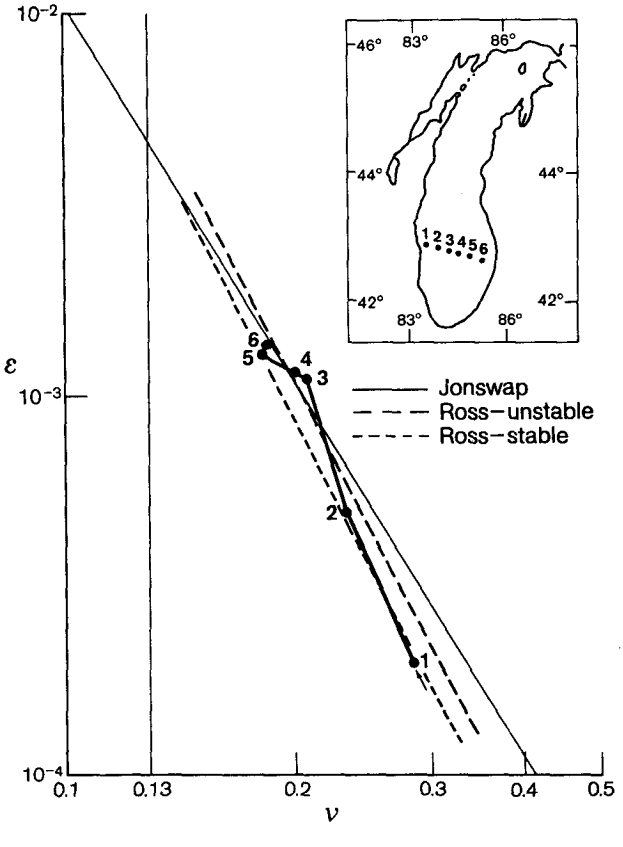

FIG. 9. As in Fig. 7 except for 1847–1900 on 21 November.

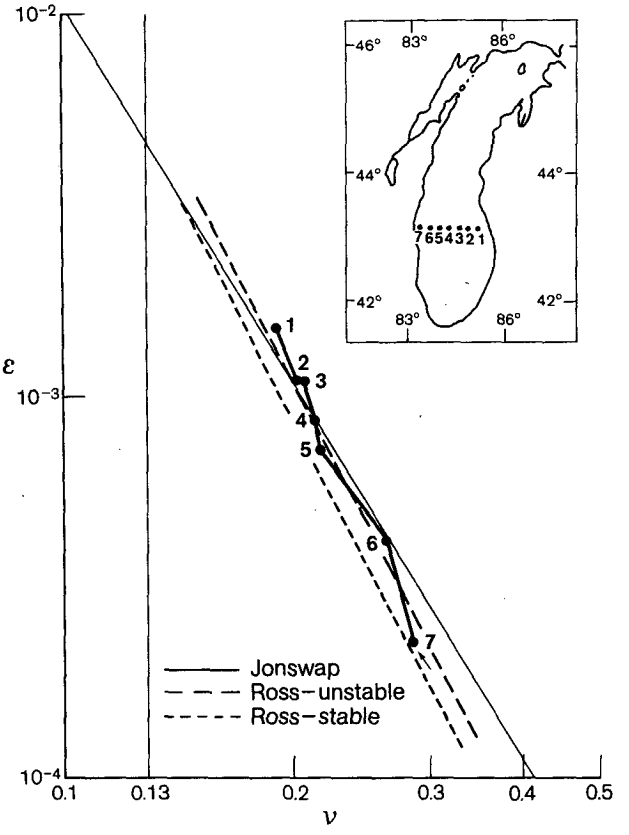

FIG. 10. As in Fig. 7 except for 1916–1932 on 21 November.

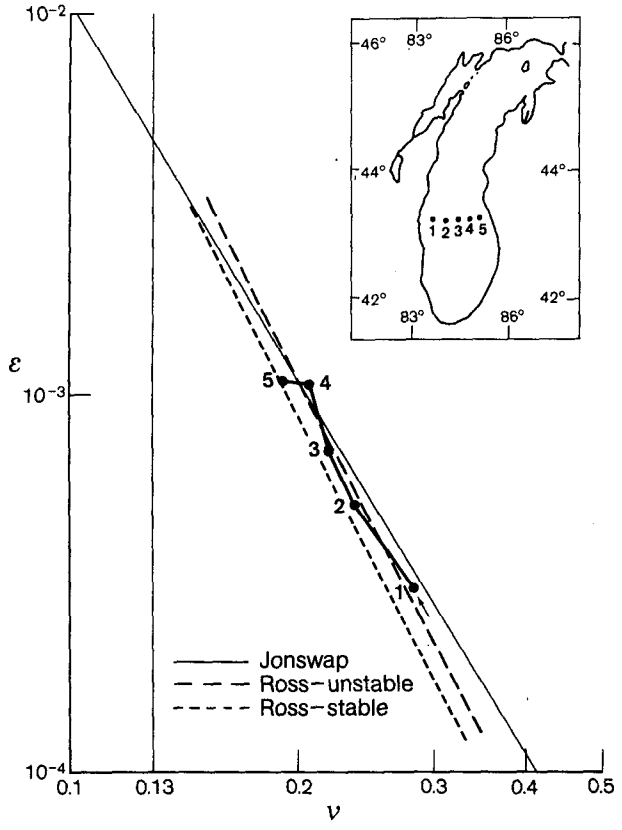

FIG. 11. As in Fig. 7 except for 2312 to 2323 on 21 November.

yet not well-understood, overshoot effect. The case of non-migration for $\nu < 0.15$ under a stable atmosphere is consistent with the open ocean data taken by DeLeonibus, Simpson, and Mattie (1974) for an air-sea temperature difference of +1.0°C.

d. Overshooting effects

In Fig. 12 we plot the growth of three low-frequency components normalized by the maximum value attained by the component during the episode versus the fetch normalized by the equivalent wavelength of the component. The figure is similar to those presented by Barnett and Sutherland (1968) and by Schule *et al.* (1971). The solid lines correspond to Fig. 7 with a long fetch and southerly wind field. The dashed lines correspond to Fig. 9 with a shorter fetch and westerly wind field.

All three frequency components were from the front face side of the wave spectra. For the 21 November case, under westerly wind across the lake, growth was basically exponential with some indication of overshoot at the higher components. For the case of southerly wind over a longer fetch on 20 November, the three components clearly displayed processes of growth and overshoot. It seems there were several stages of combined exponential growth and overshooting before reaching the saturation phase. Although some of the overshooting stages are of the size of the 90% confidence interval shown in the figure, which might cast some uncertainty, a comparison of the stages of overshoot in Fig. 12 with the loopings in Fig. 7 indicates that they approximately correspond. This crude correspondence between the stages and loops suggests that both can be conjectured as being due to the overshoot effect.

It has generally been accepted that wave growth follows four phases, as described by Phillips (1977): an initial phase of linear growth, followed by rapid exponential growth, then overshoot with subsequent oscillation, and finally saturation. The quantitative knowledge of overshoot is very limited at present. The results shown in Fig. 12, as well as the loops in Fig. 7, indicate that, for sufficiently long fetch distance under uniform wind, the process of exponential growth leading to overshoot is not a singular occurrence; rather exponential growth tends to recur after overshoot, and the process will repeat. This feature, however, is only prevalent for the lower frequency components, e.g., $f = 0.123$ Hz and to a lesser degree $f = 0.134$ Hz, and the distinction diminishes at $f = 0.146$ Hz. It seems that the four-phase wave-growth concept, while providing basic understanding of the very complicated state of the subject, may still represent an oversimplified view.

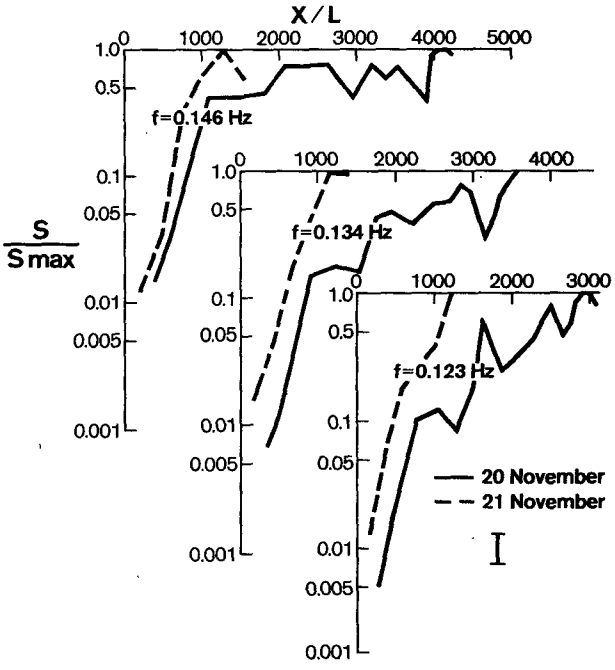

FIG. 12. Growth of spectral density with respect to fetch for three low-frequency components corresponding to the spectra of Figs. 7 and 9. The spectral density and fetch are normalized by maximum density attained and peak energy wavelength, respectively.

e. Normalization with U_*

In this study, both U_{10} and U_* were calculated simultaneously from wind measurements at flight level based on Cardone's model. The analysis presented so far has concentrated on using U_{10} rather than U_* for data normalization. This was done because 1) major results of previous studies, e.g., JONSWAP, used U_{10} for scaling, and 2) in general, U_{10} is more readily available than U_*. Hence using U_{10} will facilitate direct comparison with known results as well as practical applications. Since normalization with U_{10} leads to distinctive regimes between stable and unstable conditions, however, if stability indeed is the main effect that separates the regimes, then it can be expected that a normalization with U_* will serve to unify the regimes. As a verification of this contention, Fig. 13 presents a correlation of the nondimensionalized parameters $\xi_* = gX/U_*^2$ and $\epsilon_* = Eg^2/U_*^4$ for the five sets of wave-growth data listed in Table 1. The results clearly show that under U_* normalization the two regimes shown in Fig. 4 are no longer distinctive.

In Fig. 13, corresponding relations given in JONSWAP and by Mitsuyasu (1968) as

$$\epsilon_* = 1.6 \times 10^{-4}\xi_*, \tag{11}$$

$$\epsilon_* = 1.72 \times 10^{-4}\xi_*^{1.008}, \tag{12}$$

respectively, are also plotted as solid and dotted lines. The long dashed line denoted as "present study" is given by

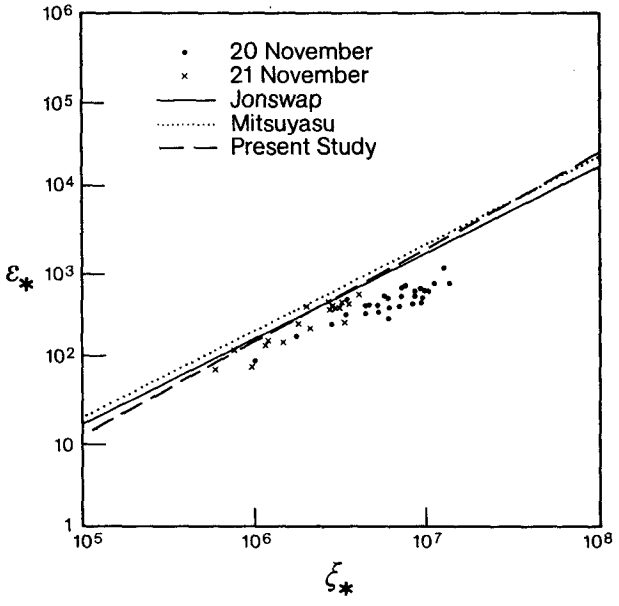

FIG. 13. Correlating ϵ_* vs ξ_* for wave growth data on 20 and 21 November.

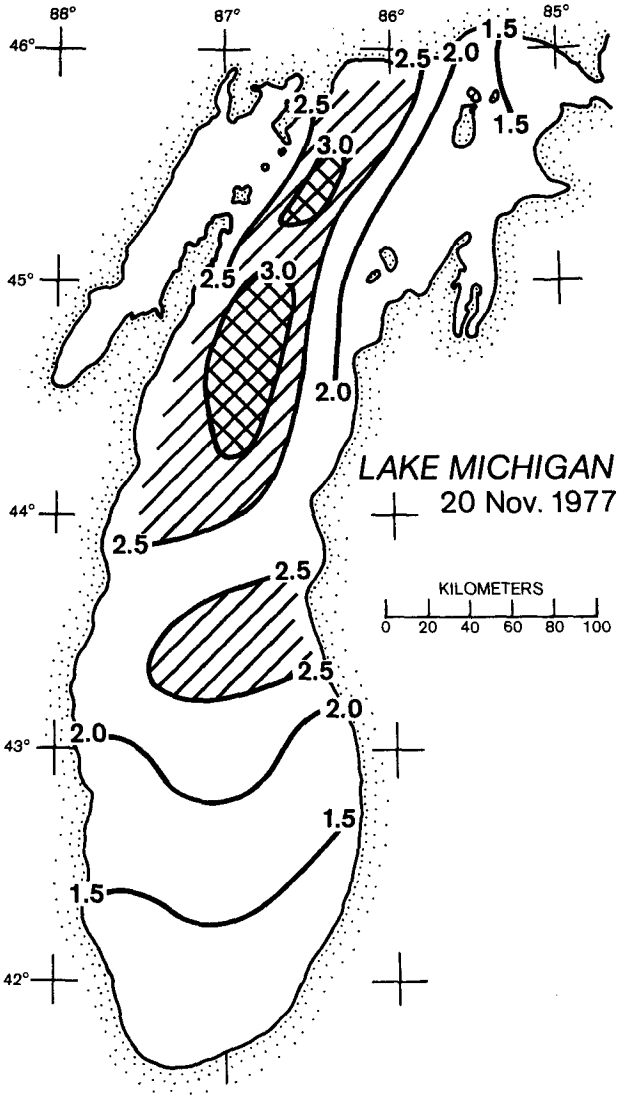

FIG. 14. Synoptic significant wave height contours for Lake Michigan during the 20 November flight.

$$\epsilon_* = 3.5 \times 10^{-5}\xi_*^{1.1}, \tag{13}$$

which was obtained by applying drag coefficients of 1.0×10^{-3} and 1.8×10^{-3}, respectively, to relations (5) and (7) to unify the stable and unstable conditions. The differences among the three ϵ_* vs ξ_* relations (11)–(13) are relatively small. They represent, however, the upper limit of the data plotted. On the other hand, the data can better fit the empirical relations with a slight reduction in the U_* value. This minor discrepancy indicates again the possible weakness in the stability parameterization used in Cardone's model. Based on the data given in Table 1, the average drag coefficient will be 1.5×10^{-3} for 20 November and 1.75×10^{-3} for 21 November. The former is certainly too high for a stable atmosphere.

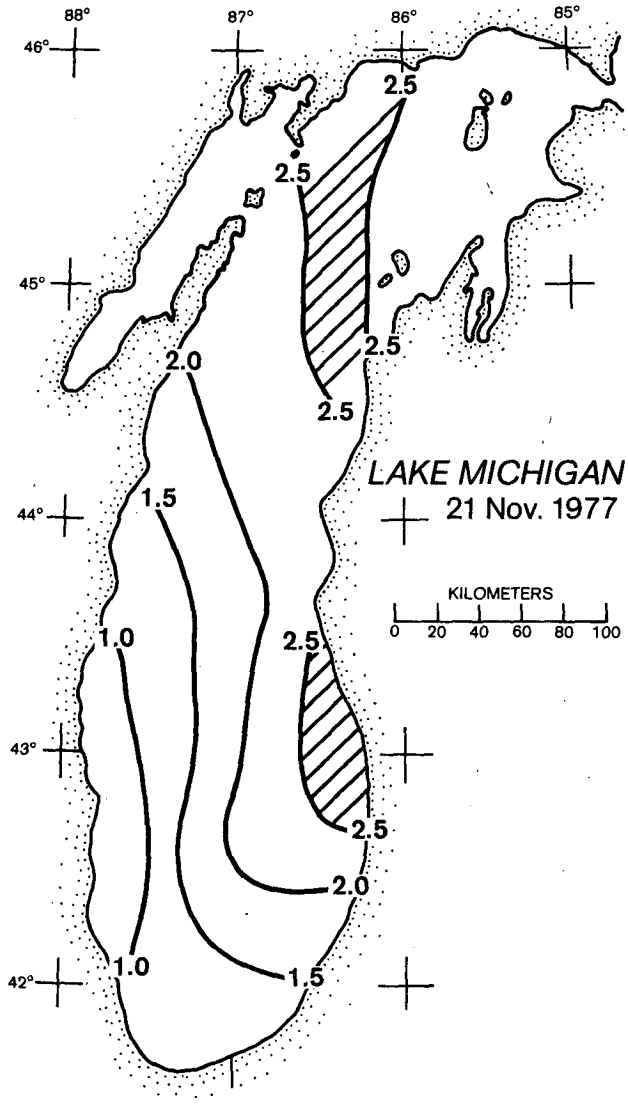

FIG. 15. As in Fig. 14 except for the 21 November flight.

f. Synoptic wave fields

One of the practical reasons for conducting this project was to examine lake-wide synoptic wave conditions. The airborne measurements during 20–21 November have provided an ideal and useful data set to achieve this purpose. With measurements spanned to cover virtually the entire lake area under a uniform wind, a synoptic wave field can be readily obtained by contouring the plotted significant wave heights at each measuring point. Figs. 14 and 15 present the Lake Michigan wave-height maps for southerly and westerly wind fields, respectively.

Examination of these wave height maps indicates that in the southern part of the lake waves behave predictably, in general, as wave heights increase in the direction of the wind with respect to fetch. On the other hand, it is difficult to provide an effective explanation for the appearance of high waves in the center region of the northern part of the lake. Conceivably, rocky shores and island chains in this area might cause attenuation due to reflections and influence the complicated behavior, which certainly deserves further exploration. For the time being, however, the availability of this kind of synoptic wave map would be very useful in selecting shipping routes under similar storm conditions.

5. Concluding remarks

Several qualitative features of wave-growth process have been presented in this paper. The results, while providing insights into the process, inadvertently demonstrated the shortcomings in the present state of wave studies. The literature has abounded with studies using a single drag coefficient to interchange U_{10} and U_* normalizations, and generally ignoring the effects of atmospheric stability. A clear distinction between the data under stable and unstable atmosphere shown in this paper, however, indicates that an accurate knowledge of the stability condition is indispensable for proper interpretation and application of the results. Such knowledge is insufficient at present. Although scaling with U_{10} has been widely used, this study strongly suggests that U_* normalization is preferable in order to cope with stability effects. This study also provided a synoptic wave-data set that leads to an overview of lake-wide characteristics of storm waves in Lake Michigan. As a first effort toward synoptic measurements of Great Lakes waves, this data set can be readily used for subsequent wave-modeling endeavors.

Acknowledgments. The authors thank C. Fred Jenkins of GLERL and lead forecasters at NWS Chicago Weather Forecast Office for providing the accurate and timely forecast required for this experiment. The suggestion to nondimensionalize wave parameters with friction velocity was made by one of the reviewers and is gratefully acknowledged.

REFERENCES

Barnett, T. P., and A. J. Sutherland, 1968: A note on an overshoot effect in wind-generated waves. *J. Geophys. Res.*, **73**, 6879–6885.

——, and J. C. Wilkerson, 1967: On the generation of ocean wind waves as inferred from airborne radar measurements of fetch-limited spectra. *J. Mar. Res.*, **25**, 292–328.

Blackman, R. B., and J. W. Tukey, 1958: *The Measurement of Power Spectra*. Dover, 190 pp.

Cardone, V. J., 1969: Specification of the wind distribution in the marine boundary layer for wave forecasting. Rep. TR-69-1, Contract NONR 285(57), Dept. Meteor. Oceanogr., New York University, 131 pp. [NTIS AD-702 490].

DeLeonibus, P. S., L. S. Simpson and M. G. Mattie, 1974: Equilibrium range in wave spectra observed at an open-ocean tower. *J. Geophys. Res.*, **79**, 3041–3053.

Hasselmann, K., 1978: On the spectral energy balance and numerical prediction of ocean waves. *Turbulent Fluxes Through the Sea Surface, Wave Dynamics, and Prediction*, A. Favre and K. Hasselmann, Eds., Plenum Press, 531–545.

——, D. B. Ross, P. Muller and W. Sell, 1976: A parametric wave prediction model. *J. Phys. Oceanogr.*, **6**, 200–228.

——, T. P. Barnett, E. Bouws, H. Carlson, D. E. Cartwright, K. Enke, J. A. Ewing, H. Gienapp, D. E. Hasselmann, P. Kruseman, A. Merrburg, P. Miller, D. J. Olbers, K. Richter, W. Sell and H. Walden, 1973: Measurements of wind-wave growth and swell decay during the Joint North Sea Wave Project (JONSWAP). *Dtsch. Hydrogr. Z. Ergängzungsheft* **A12**, 95 pp.

Kitaigorodski, S. A., 1962: Applications of the theory of similarity to the analysis of wind-generated wave motion. *Izv., Geophys. Ser. Acad. Sci.*, USSR, **1**, 105–117.

Liu, P. C., and R. J. Robbins, 1974: Wave data analyses at GLERL. *Proc. Int. Symp. Ocean Wave Measurement and Analyses*, Vol. 1, Amer. Soc. Civil Eng., 64–73.

Mitsuyasu, H., 1968: On the growth of the spectrum of wind-generated waves (I). *Rep. Res. Inst. Appl. Mech., Kyushu Univ.*, **16**, 459–482.

Phillips, O. M., 1977: *The Dynamics of the Upper Ocean*, 2nd ed. Cambridge University Press, 336 pp.

Ross, D. B., 1978: On the use of aircraft in the observation of one- and two-dimensional ocean wave spectra. *Ocean Wave Climate*, M. D. Earle and A. Malahoff, Eds., Plenum Press, 253–267.

——, and V. J. Cardone, 1974: Observations of oceanic whitecaps and their relation to remote measurements of surface wind speed. *J. Geophys. Res.*, **79**, 444–452.

——, —— and J. W. Conaway, Jr., 1970: Laser and micro wave observations of sea-surface conditions for fetch-limited 17- to 25-m/s winds, *IEEE Trans.*, **GE-8**, 326–336.

Schule, J. J., L. S. Simpson and P. S. DeLeonibus, 1971: A study of fetch-limited wave spectra with an airborne laser. *J. Geophys. Res.*, **76**, 4160–4171.

Wilkerson, J. C., and J. F. Ropek, 1967: An application of Naval oceanographic development to inland waters. *Proc. Tenth Conf. Great Lakes Res.*, Toronto, Int. Assoc. Great Lakes Res., 456–460.